IOPscience iopscience.iop.org

Home Search Collections Journals About Contact us My IOPscience

Magnetic properties of tapiolite ($FeTa_2O_6$); a quasi two-dimensional (2D) antiferromagnet

This article has been downloaded from IOPscience. Please scroll down to see the full text article.

2004 J. Phys.: Condens. Matter 16 7837

(http://iopscience.iop.org/0953-8984/16/43/023)

View the table of contents for this issue, or go to the journal homepage for more

Download details:
IP Address: 129.252.86.83
The article was downloaded on 27/05/2010 at 18:24

Please note that terms and conditions apply.

INSTITUTE OF PHYSICS PUBLISHING JOURNAL OF PHYSICS: CONDENSED MATTER

J. Phys.: Condens. Matter **16** (2004) 7837–7852 PII: S0953-8984(04)79761-1

Magnetic properties of tapiolite ($FeTa_2O_6$); a quasi two-dimensional (2D) antiferromagnet

E M L Chung[1], M R Lees[1], G J McIntyre[2], C Wilkinson[2,3], G Balakrishnan[1], J P Hague[4], D Visser[5] and D McK Paul[1]

[1] Department of Physics, University of Warwick, Coventry CV4 7AL, UK
[2] Institut Laue Langevin, BP 156, 38042, Grenoble Cedex 9, France
[3] Department of Chemistry, University of Durham, Durham DH1 3LE, UK
[4] Department of Physics and Astronomy, University of Leicester, Leicester LE1 7RH, UK
[5] Rutherford Appleton Laboratory, Didcot, Oxfordshire OX11 OQX, UK

E-mail: james.hague1@alumni.jesus.ox.ac.uk

Received 21 April 2004
Published 15 October 2004
Online at stacks.iop.org/JPhysCM/16/7837
doi:10.1088/0953-8984/16/43/023

Abstract

The possibilities of two-dimensional (2D) short-range magnetic correlations and frustration effects in the mineral tapiolite are investigated using bulk-property measurements and neutron Laue diffraction. In this study of the magnetic properties of synthetic single-crystals of tapiolite, we find that single crystals of $FeTa_2O_6$ order antiferromagnetically at $T_N = 7.95 \pm 0.05$ K, with extensive two-dimensional correlations existing up to at least 40 K. Although we find no evidence that $FeTa_2O_6$ is magnetically frustrated, hallmarks of two-dimensional magnetism observed in our single-crystal data include: (i) broadening of the susceptibility maximum due to short-range correlations, (ii) a spin-flop transition and (iii) lambda anomalies in the heat capacity and $d(\chi T)/dT$. Complementary neutron Laue diffraction measurements reveal 1D magnetic diffuse scattering extending along the $\mathbf{c}^*$ direction perpendicular to the magnetic planes. This magnetic diffuse scattering, observed for the first time using the neutron Laue technique by VIVALDI, arises directly as a result of 2D short-range spin correlations.

1. Introduction

Named after the god Tapio of Finnish mythology, tapiolite ($FeTa_2O_6$) is a naturally occurring mineral, and one of a group of compounds possessing the general formula $A^{2+}B_2^{5+}O_6$. Although it is possible to find natural single crystals of tapiolite growing in granite pegmatites, these tend to contain impurities such as Mn^{2+} and Nb^{2+}, and exhibit a substantial reduction in cation ordering. Previous reports of the magnetic properties of $FeTa_2O_6$ have therefore been confined to the study of high-purity polycrystalline samples, in which low-dimensional

 © 2004 IOP Publishing Ltd Printed in the UK

magnetic properties tend to be obscured by the averaging effects of the powder sample [1, 2]. Recently, we have succeeded in growing large high-purity artificial single crystals of $FeTa_2O_6$ using the floating-zone method, under simpler conditions than published previously (section 2). This progress has enabled us to examine the magnetic properties of *single crystals* of $FeTa_2O_6$, paying particular attention to low-dimensional magnetic behaviour and possible frustration effects [3]. During the course of our investigations we chart the bulk magnetic properties of $FeTa_2O_6$ single crystals, and reveal several interesting features of low-dimensional magnetism not previously visible in polycrystalline samples.

Low-dimensional magnetism has been of particular interest in recent years. Quasi-2D materials such as the superconducting cuprates and some CMR manganites are of immense technological importance, and a significant effort from both theorists and experimentalists has been directed at unlocking the mechanisms underpinning their behaviour. $FeTa_2O_6$ is an alternative example of a low-dimensional magnet. As we demonstrate here, it is an $S = 2$ system, which makes it a good system for modelling. It has a relatively complicated unit cell structure, which is expected to lead to interesting microscopic mechanisms for magnetism. Also, the material changes between 2D and 3D magnetic behaviour at a moderate temperature, and this makes the material an ideal candidate for Laue diffraction using VIVALDI, the first instrument of the ILL's Millennium Program.

We find that heat capacity (section 3), magnetization (section 4) and neutron scattering (section 5) measurements are consistent with an antiferromagnetic ordering temperature of $T_N = 7.95 \pm 0.05$ K. Lambda anomalies observed in the magnetic heat capacity and $\mathrm{d}(\chi T)/\mathrm{d}T$ indicate that short-range correlations are important up to at least 40 K. The magnetic entropy (section 3.1) shows that the spins in $FeTa_2O_6$ are $S = 2$, and that approximately 73% of the magnetic entropy associated with the disordering of the spins is lost through short-range ordering at temperatures in excess of T_N.

Our magnetization measurements confirm that the ordered antiferromagnetic structure of $FeTa_2O_6$ is composed of collinear $\langle 110 \rangle$ spins lying in the a–b plane. The presence of perpendicular sets of spins is also confirmed by the behaviour of a spin-flop transition observed at $T = 1.6$ K, $H = 70$ kOe, and a qualitative model for the spin flop is proposed (section 4.3). No evidence for the frustration or 1D short-range order in $FeTa_2O_6$ was found.

Lastly, the 2D nature of the short-range correlations in $FeTa_2O_6$ are revealed with striking clarity using neutron-Laue diffraction [4] (section 5). Streaks observed in the difference Laue diffraction pattern at 8 K correspond to the projections of 1D diffuse rods that extend perpendicular to the magnetic planes along $\mathbf{c}^*$. These diffuse scattering rods arise as a direct result of the presence of 2D short-range magnetic order.

1.1. Chemical and magnetic structure

The trirutile crystal structure of $FeTa_2O_6$ (space group symmetry $P4_2/mnm$) was first discovered during a study of the mineral tapiolite by Goldschmidt in 1926 [5]. Stacking of divalent and pentavalent cations along the c-axis results in a chemically ordered network of interpenetrating edge and corner-sharing octahedra [6], as shown in figure 1. The octahedra are slightly distorted due to a static Jahn-Teller effect and possess apical oxygen atoms oriented along [110] and $[\bar{1}10]$ directions in alternate planes.

The Fe^{2+} sublattice in $FeTa_2O_6$ possesses the same symmetry as the Ni^{2+} sublattice in the well-known two-dimensional Heisenberg antiferromagnet, K_2NiF_4 [7]. By symmetry arguments, interactions between adjacent magnetic layers are shown to be negligible. Meanwhile, next-neighbouring layers are weakly interacting, since the superexchange interaction is short-ranged and mediated through three intervening O anions and two Ta cations.

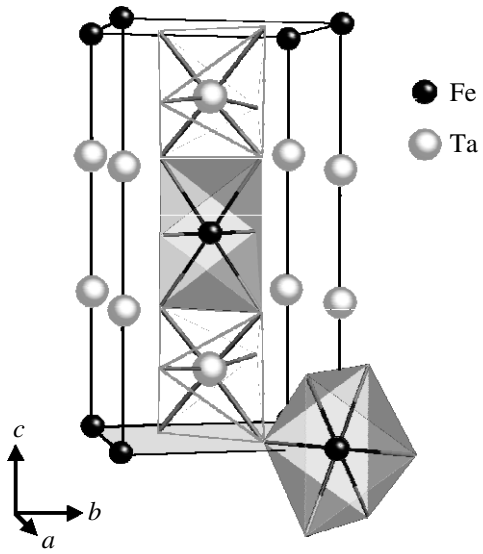

Figure 1. $FeTa_2O_6$ chemical unit cell (containing 18 atoms). Fe and Ta atoms are positioned at the centre of O octahedra. (Fe–O groups are shaded.) Oxygen atoms positioned at the vertices are shared between adjacent octahedra.

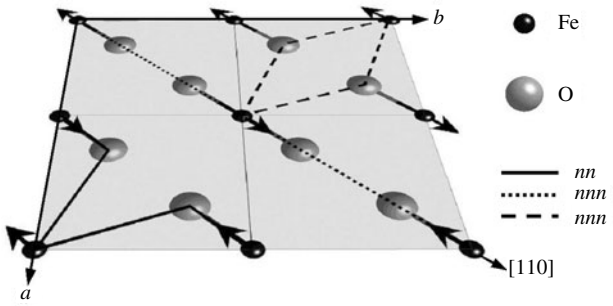

Figure 2. The {001} basal plane of four unit cells of $FeTa_2O_6$, illustrating intra-plane nearest-neighbour (*nn*) and next-nearest-neighbour (*nnn*) exchange pathways. Arrows indicate the directions of the magnetic moments.

In $FeTa_2O_6$, the inter-plane interactions are therefore expected to be several orders of magnitude smaller than in-plane interactions and the chemical structure supports the existence of two-dimensional magnetic behaviour and short-range correlation effects.

1.2. Intra-layer interactions

The intralayer exchange pathways in $FeTa_2O_6$ are more convoluted than in K_2NiF_4 due to an asymmetric arrangement of bridging oxygen atoms. The nearest-neighbour (*nn*) and multiple next-nearest-neighbour (*nnn*) exchange pathways, superposed upon the accepted magnetic structure of four unit cells of $FeTa_2O_6$, are shown in figure 2. Competition between intralayer exchange interactions leads to the possibility of short-range one-dimensional correlations and magnetic frustration effects. Similar effects were recently suggested to play an important role in explaining the complex magnetic structure of the isostructural compound $CrTa_2O_6$

[3]. Although inspection of the ordered magnetic structure of $FeTa_2O_6$ indicates that *nnn* exchange interactions are dominant, it is difficult to distinguish whether it is the linear *nnn* superexchange along the [110] Fe–O–O–Fe direction, or the 160° [$\bar{1}$10] Fe–O–Fe interaction that is most important.

1.3. Previous work

The magnetic structure of $FeTa_2O_6$ has previously been investigated using Mössbauer spectroscopy [1, 2, 8], and powder neutron-diffraction measurements [2, 9]. These studies suggest that the spins in $FeTa_2O_6$ are constrained to the *a*–*b* plane, with each layer consisting of a collinear arrangement of moments where opposite spins are oriented along ±[110] directions, as shown in figure 2. Although it is known that the layers stack antiferromagnetically in the **c**-direction, the exact configuration of the 3D magnetic structure remains ambiguous.

Past reports of the bulk magnetic properties of $FeTa_2O_6$ have been based exclusively upon the analysis of polycrystalline samples. Early researchers mistakenly report the long-range ordering temperature of $FeTa_2O_6$ as coinciding with the maximum in the susceptibility at $T(\chi_{max}) \simeq 14$ K [8, 10]. In fact, a single thermodynamic quantity is not sufficient to characterize the system fully, and measurements of other properties such as the heat capacity are required to show that the true Néel temperature of $FeTa_2O_6$ occurs at around $T_N = 8$ K [2, 11].

$FeTa_2O_6$ powder susceptibility data [2] have been modelled by Muraoka *et al* [12] by fitting to the Padé approximated high-temperature expansion of a two-dimensional anisotropic Heisenberg model with $S = 2$ spins placed on a square lattice:

$$H = -2J \sum_{\langle i,j \rangle}^{nn} \mathbf{S_i} \cdot \mathbf{S_j} - 2\alpha J \sum_{\langle i,j \rangle}^{nnn} \mathbf{S_i} \cdot \mathbf{S_j} - D \sum_i \mathbf{S}_{iz}^2. \tag{1}$$

The first two terms represent *nn* and *nnn* Heisenberg intra-plane exchange interactions, see figure 2. The *nn* and *nnn* exchange constants are denoted by J and J', with their ratio defined as $\alpha = J'/J$. The third term represents the 'z-axis' single-ion anisotropy, forcing spins to lie along the 'z-axis' with stiffness D. It should be made clear that the z-axis in this model for $FeTa_2O_6$ is directed along the [110] Fe^{2+}–O^{2-} bond, along which the moments are thought to align, and does not correspond to the c-axis.

Muraoka *et al* obtain the following results: $-0.41 \leqslant J/k_B \leqslant -0.39$ K, $0.6 \leqslant \alpha \leqslant 0.9$ and $6.7 \leqslant D/k_B \leqslant 7.1$ K. Since the single-ion anisotropy is large, the behaviour of $FeTa_2O_6$ in some ways resembles that of a 2D Ising system. The phase diagram for the fustrated 2D Ising model at 0 K has been examined by Fan and Wu [13] who found that the '*super-antiferromagnetic*' configuration, exhibited by $FeTa_2O_6$, will be realized as the ground state structure only if $-|J| > 2J'$. This condition is consistent with the values obtained by Muraoka *et al* from their suseptibility analysis [12].

2. Sample preparation

Stoichiometric quantities of $Fe(COO)_2{\cdot}nH_2O$ and Ta_2O_5 (both 99.99% purity) were mixed in ethanol, dried and pre-heated at 1000 °C for 1.5 h under a gas flow of 50 ml min^{-1} of argon. The resulting orange powder was then pressed into cylindrical rods and sintered at 1400 °C for 2 h under the same conditions as the initial firing.

The growth of large single-crystal specimens of $FeTa_2O_6$ was performed using a commercial four-ellipsoid optical floating-zone furnace. We followed a similar technique

Figure 3. $FeTa_2O_6$ crystalline boule grown by the floating-zone method at 1.5 mm h^{-1} in 1 atm of Ar + 3% H. The crystal is approximately 4 cm in length.

to that published by Tanaka *et al* [14], except that the controlled atmosphere of Ar, CO and CO_2 was replaced by a simple gas mixture of Ar and 3% H.

The chamber of the furnace was evacuated to a vacuum better than 1×10^{-5} Torr and a gas of Ar and 3% H introduced to a pressure of 1 atm. The growth rate was stabilized at 1.5 mm h^{-1}, with the feed and seed rods rotated at 25–30 rpm.

Several large dark grey single-crystals of $FeTa_2O_6$ possessing a metallic lustre were obtained (figure 3). Growth striations and two extended large facets separated by 180° were visible along the entire length of the boule. X-ray Laue photographs confirmed the tetragonal symmetry of the crystal, and indicated that the growth direction adopted was roughly along the ⟨103⟩. Both x-ray and neutron Laue photographs indicate the $FeTa_2O_6$ single crystals to be of exceptional quality and low mosaic spread (see section 5).

Powder x-ray diffraction patterns were obtained at room temperature using a standard laboratory diffractometer with monochromatic Cu K_α radiation ($\lambda = 1.540(6)$ Å). The powder pattern collected for small portions of finely crushed single crystal indicated our samples to be of excellent purity. All peaks were indexed in the tetragonal space group $P4_2/mnm$. The observed lattice parameters ($a = b = 4.75(6)$ Å, $c = 9.18(9)$ Å) are in general agreement with previously published reports [6, 14]. Our samples had a density of 8.4 ± 0.5 g cm^{-3}, which compares favourably to the density of 8.2 ± 0.2 g cm^{-3} calculated from the measured lattice parameters. Magnetization and neutron scattering measurements were performed using the same 53 mg $FeTa_2O_6$ single crystal cut with [001] faces 3.2 mm apart, and parallel sets of [1.82 0.85 0] and [−1.54 1.29 0] faces spaced approximately 2.4 mm apart. To ensure good thermal contact, heat capacity measurements were performed using flat discs of $FeTa_2O_6$ crystal of weight 96 and 156 mg both 5 mm in diameter.

3. Heat capacity

The results of heat-capacity measurements performed on the 96 and 156 mg $FeTa_2O_6$ crystals using a standard calorimetric relaxation technique between 2 and 250 K are presented in figure 4. A lambda anomaly was observed at $T_N = 8.0 \pm 0.05$ K, signalling the onset of long-range magnetic order (see figure 5). Table 1 contains values for T_N obtained by this and previous heat capacity and susceptibility measurements.

Previous heat capacity measurements, performed on polycrystalline $FeTa_2O_6$, were conducted over a less-extensive temperature range, from 2 to 60 K by Eicher *et al* [2], and from 2 to 24 K by Zawislak *et al* [11]. In this study, the temperature range of the data extends from 2 to 250 K, which allows a more detailed analysis of the magnetic contribution to the heat capacity to be performed. The magnetic heat capacity was extracted by subtraction of the phonon component arising from vibrations of the crystalline lattice. To estimate the phonon contribution, the high temperature data from 50 to 250 K were fitted to the following

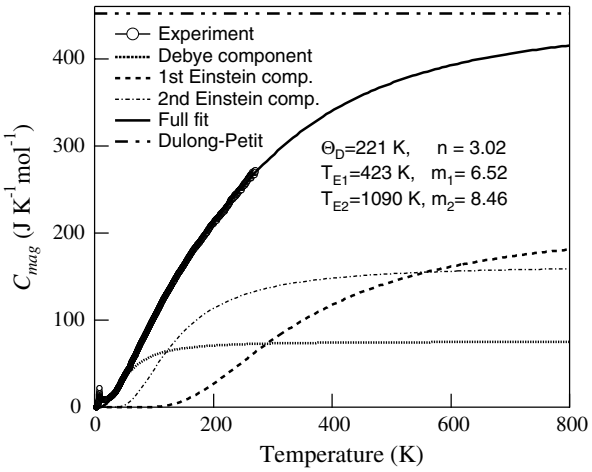

Figure 4. $FeTa_2O_6$ heat capacity data obtained for 96 and 156 mg crystals of $FeTa_2O_6$ in zero-field between 2 and 250 K. ○, observed data; —, fit obtained by using the Debye–Einstein scheme; - - -, Debye contribution; and – – –, Einstein contribution. Fitting has been performed between the low-temperature point of inflection at ∼30 K and the maximum measured temperature of 250 K.

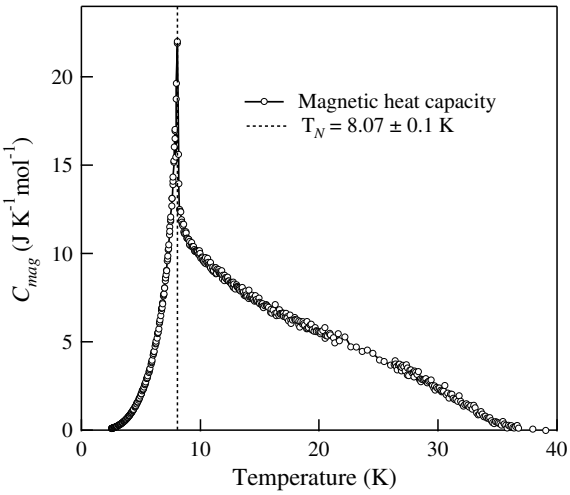

Figure 5. The estimated magnetic contribution to the heat capacity C_{mag} from $FeTa_2O_6$.

Debye–Einstein expression:

$$C_{\text{lat}} = 3R\left[nC_{\text{Debye}}(\theta_D/T) + \sum_i m_i C_{\text{Einstein}}(T_{Ei}/T)\right]. \tag{2}$$

The Debye integral was evaluated numerically via the trapezium method. R is the gas constant and θ_D and T_{Ei} denote the Debye and Einstein temperatures. The Debye component represents acoustic phonon modes and low-energy optical modes with strong dispersion in the second Brillouin zone, while the Einstein component is characteristic of higher-energy optical modes with almost flat dispersion. Multiple Einstein modes are expected, since the complexity of the unit cell will lead to many optical phonons. At temperatures in excess of θ_D and T_E, all modes

Table 1. Values for T_N and $T(\chi_{max})$ for an $FeTa_2O_6$ single-crystal (this work) and a polycrystalline $FeTa_2O_6$ (previous work).

Group	T_N (K)	$T(\chi_{max})$ (K)
This work ⟨001⟩	8 ± 0.05	8.7 ± 0.1
This work ⟨110⟩	8 ± 0.05	14.7 ± 0.1
Zawislak *et al* [1]	8	8.7 ± 0.2
Takano *et al* [8]	–	14
Eicher *et al* [2]	8.5	15
Bernier *et al* [10]	–	13

are stimulated and the lattice heat capacity is predicted (according to the law of Dulong and Petit) to saturate with a total number of modes given by $3(n + \sum_i m_i)R$, where $n + \sum_i m_i = 18$ is the effective number of atoms per unit cell. (This value is twice the actual number of atoms per formula unit, because the structural distortion associated with the oxygen tetrahedra doubles the size of the unit cell.)

Although our heat capacity measurements do not reach high enough temperatures to excite all of the phonons, the Dulong–Petit law suggests that the lattice heat capacity saturates at a value of at least $440\ \mathrm{J\ K^{-1}\ mol^{-1}}$ (figure 4).

We found that two Einstein modes were essential to fit the data. Any additional modes only lead to slight improvements to the fit, and cause minor changes to the Debye temperatures of the most important contributions. From the fit shown in figure 4 we obtain Debye and Einstein parameters of $n = 3.02$, $\theta_D = 221$ K, $m_1 = 6.52$, $T_{E1} = 423$ K and $m_2 = 8.46$, $T_{E2} = 1090$ K. Although we found that it was not possible to fit the whole data set using a single Debye curve, below $T \sim 60$ K where the magnetic heat capacity is largest, the lattice component is dominated almost entirely by the Debye contribution.

The estimated magnetic heat capacity of $FeTa_2O_6$ is displayed in figure 5. This has been calculated by subtraction of the fitted Debye–Einstein curve. Asymmetry characterized by the slow decay of the magnetic lambda-peak provides a good indication of the existence of strong short-range order (SRO) effects above T_N. SRO was seen to extend from T_N to ∼35 K.

3.1. Magnetic entropy

The molar magnetic entropy (S_m) of $FeTa_2O_6$, was calculated from the estimated magnetic heat capacity via numerical integration:

$$S_m = \int_0^T \frac{C_{mag}}{T}\,\mathrm{d}T. \tag{3}$$

A plot of the temperature dependence of the unnormalized magnetic entropy (left axis, —), and C_{mag}/T (right axis, markers), is displayed in figure 6. A large proportion of the molar magnetic entropy increase on warming the sample is gained above T_N. At the Néel temperature, the magnetic entropy is equal to $S_m = 3.67\ \mathrm{J\ K^{-1}\ mol^{-1}}$, which corresponds to only 27% of the saturation value. This implies that 73% of the magnetic entropy disappears at temperatures above T_N via short-range ordering effects.

The asymptotic value of the magnetic heat capacity as T tends to infinity is given theoretically by $S_m = R\ln(2S + 1)$. Disordering of $S = 1/2$ and $S = 2$ spins would produce asymptotic values for the molar magnetic entropy of $S_m = 5.74$ and 13.34, respectively. It is clear from figure 6 that the entropy saturates at almost exactly the value expected for a

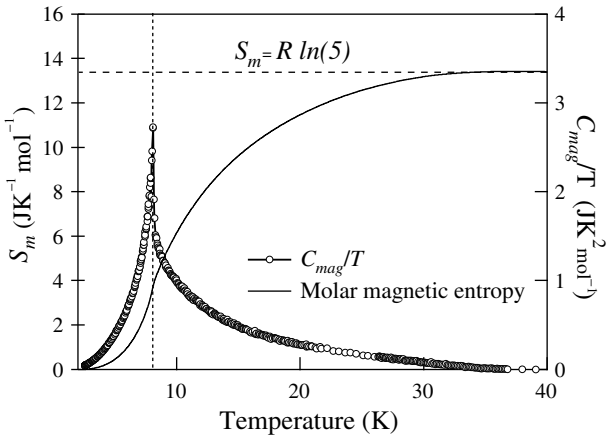

Figure 6. $FeTa_2O_6$ molar magnetic entropy (lhs scale, —). The rhs axis shows C_{mag}/T prior to integration (markers). The dashed horizontal line indicates the asymptotic value of the magnetic heat capacity predicted for a system of $S = 2$ spins.

compound with a spin state of $S = 2$. We find no evidence to confirm the existence of a mixed spin state in $FeTa_2O_6$.

4. Magnetization measurements

Susceptibility data was obtained in the range 4–300 K at a field of $\mathbf{H} = 1$ kOe using a superconducting quantum interference device (SQuID) magnetometer. **M**–**H** curves in fields up to 100 kOe were measured using a vibrating-sample magnetometer (VSM). The angle between the *c*-axis of the crystal and the applied field in both magnetometers was controlled to better than $\pm 4^\circ$. Rotation of the crystal within the *a*–*b* plane could be achieved using a rotating sample holder within an accuracy of $\pm 7^\circ$. The crystal was fixed to the holder using a particularly strong cold resistant adhesive, since it was noted to experience a substantial torque during spin reorientation.

4.1. Susceptibility data

The crystal was oriented with **H** directed along the $\langle 110 \rangle$ and $\langle 001 \rangle$ directions. The results obtained at 1 kOe are shown in figure 7(a). Differences between the $\mathbf{H} \| \langle 001 \rangle$ and $\mathbf{H} \| \langle 110 \rangle$ curves are indicative of high anisotropy between the *a*–*b* plane and the *c*-direction.

In comparison to previous studies performed upon polycrystalline materials (see table 1), our single-crystal data show a clear point of inflexion at $T_N = 8.0 \pm 0.1$ K. Above T_N, short-range correlations in the *a*–*b* plane give rise to a broad maximum $d\chi/dT = 0$) in the susceptibility at $T(\chi_{max})$. Broadening of the susceptibility maximum arises from short-range correlations, and represents a classic signature of 2D magnetic systems. Indeed, the ratio $T_N/T(\chi_{max})$ is often used to measure the extent of these low-dimensional correlations for comparison of one material to another [7]. An explicit relationship between the magnetic heat capacity and susceptibility measurements has been established by Fisher in 1962 [15], who found that a maximum in χ close to the discontinuity in the heat capacity portrays a rapid decay of short-range order above T_N.

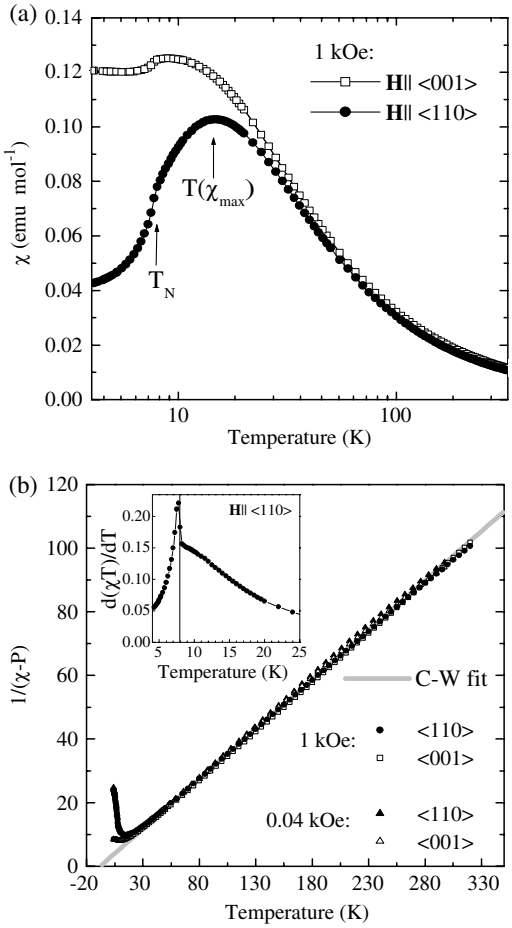

Figure 7. (a) $FeTa_2O_6$ susceptibilty data collected at 1 kOe along the ⟨110⟩ and ⟨001⟩ directions. (b) Data collected at 0.04 and 1 kOe plotted as $1/(\chi - P)$. P represents a small positive constant, see table 2. The inset shows $\mathrm{d}(\chi T)/\mathrm{d}T$.

In $FeTa_2O_6$, we find the ratio $T_N/T(\chi_{max})$ is crucially dependent upon the orientation of the crystal relative to **H**. For $\mathbf{H}\|\langle 001\rangle$, $T_N/T_{max} = 0.92 \pm 0.03$, while for $\mathbf{H}\|\langle 110\rangle$, $T_N/T_{max} = 0.54 \pm 0.02$. This provides evidence that short-range order is most prevalent within the *a–b* plane.

A plot of the derivative of χT for the ⟨110⟩ direction is provided in figure 7(b, inset). This quantity $(\mathrm{d}(\chi T)/\mathrm{d}T) = \chi + T\,\mathrm{d}\chi/\mathrm{d}T)$ has been chosen since it is directly representative of the magnetic contribution to the heat capacity, C_{mag}, plotted in figure 5. C_{mag} and $\mathrm{d}(\chi T)/\mathrm{d}T$ for the ⟨110⟩ direction are in good qualitative agreement. Above T_N, both quantities exhibit a slow decay, which is consistent with short-range ordering in the *a–b* plane.

Each set of data provided a satisfactory fit to the Curie–Weiss equation

$$\frac{1}{(\chi - P)} = \frac{(T - \theta_P)}{C}, \tag{4}$$

where C is the Curie constant, P is a small positive correction and θ_P is the Curie temperature. The results of fits to the data are presented in table 2 and figure 7(b). Previous results (for comparison) are presented in table 3. The uncertainties quoted in the table are inclusive of

Table 2. Curie–Weiss parameters for the $FeTa_2O_6$ single crystal (this work).

Direction	Field (kOe)	P (emu)	$\mu_{eff} \pm 0.05\mu_B$	$\theta_p \pm 1$ (K)
⟨001⟩	0.04	0.0124	5.07	−8.0
⟨110⟩	0.04	0.0079	5.02	−8.3
⟨001⟩	1	0.0018	5.12	−8.1
⟨110⟩	1	0.0009	5.10	−9.3

Table 3. Polycrystalline $FeTa_2O_6$ Curie–Weiss parameters (previous work).

Group	Field (kOe)	$\mu_{eff} \pm 0.05\mu_B$	$\theta_p \pm 1$ (K)
Zawislak *et al* [11]	–	5.06	−8.7
Takano *et al* [8]	40, 50, 82	4.9	−8
Eicher *et al* [2]	1.5	5.03	−11
Bernier *et al* [10]	–	5.12	−16

variations introduced by the selective nature of the temperature range used in the fit. Values obtained for the molar Curie constant, $C_M = 3.2\,\mathrm{cm^3\,K\,mol^{-1}}$, correspond to an effective Fe^{2+} moment of around $5\mu_B$. This compares favourably to the value of $4.9\mu_B$ calculated by assuming $J = S$ (i.e. quenching of the orbital angular momentum). The paramagnetic Curie temperature obtained from our fitting was around $\theta_p = -8.3$ K, confirming that the interactions in $FeTa_2O_6$ are antiferromagnetic. As $|\theta_p|$ is comparable in magnitude to T_N we conclude that little frustration is present in this structure.

4.2. M–H loops

M–**H** curves obtained at temperatures between 1.6 and 20 K with $\mathbf{H}\|\langle 110\rangle$ and $\mathbf{H}\|\langle 001\rangle$ are presented in figures 8 and 9, respectively. The magnetization curves obtained with **H** applied along perpendicular directions within the *a*–*b* plane were identical within the limits of our experiment, confirming that the bulk sample contains roughly equal populations of perpendicular moments.

In the ⟨001⟩ direction, the **M**–**H** dependence remains roughly linear even below T_N (figure 8). This corresponds to a gradual alignment of the moments with increasing field by tilting out of the plane. In the ⟨110⟩ direction at 1.6 K, a spin-flop transition is observed at a critical field of $H_{SF} = 69 \pm 1$ kOe (figure 9). A smaller feature, associated with a very small amount of hysteresis (not visible on the scale of the graph), is also observed at $H \simeq 47$ kOe. This feature suggests that at 47 kOe the spins begin to flop. It is possible that the hysteresis occurs due to a slight reconfiguration of magnetic domains.

Above T_N, the ⟨110⟩ data retain a slight inverse curvature. This is at variance with the Brillouin function typically associated with the saturation of a 3D paramagnet, and is probably due to the effects of reduced dimensionality of the magnetic interactions.

4.3. The spin-flop transition

In uniaxial antiferromagnets, such as MnF_2, a sharp rise in the magnetization corresponding to a spin-flop transition has been observed and has been well-characterized [7, 16]. The spin-flop is first order when **H** is applied parallel to the spin direction, and occurs at a critical field, H_{SF}. During the spin-flop process the staggered magnetization $\mathbf{L} = \mathbf{M}_1 - \mathbf{M}_2$, given by subtraction of the magnetization of each of the antiferromagnetic sublattices, rotates to become perpendicular to **H**.

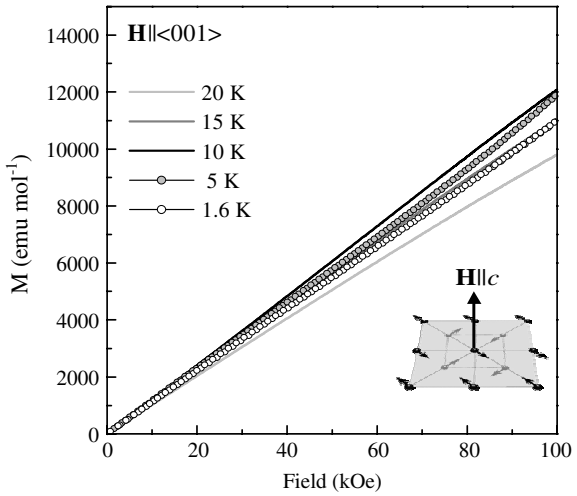

Figure 8. Variation of magnetization with applied field for a $FeTa_2O_6$ single crystal oriented with **H** parallel to ⟨001⟩. Data were obtained at temperatures of 1.6, 5, 10, 15 and 20 K, with the crystal warmed to at least 20 K and then zero-field cooled between each measurement. The data shown include both the virgin and the return cycles of the curve.

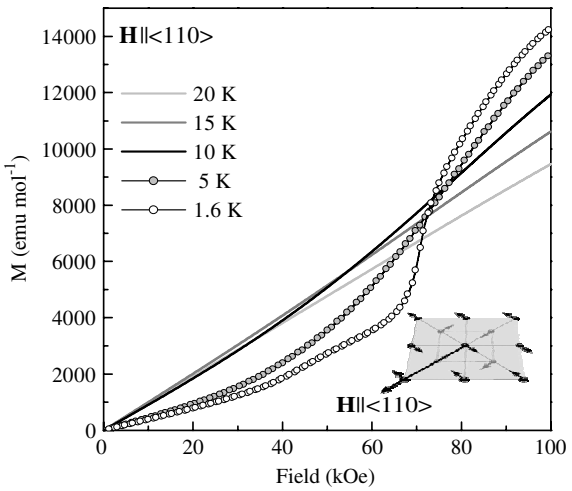

Figure 9. Variation of magnetization with applied field for a $FeTa_2O_6$ single-crystal orientated with **H** parallel to ⟨110⟩. Data were obtained at temperatures of 1.6, 5, 10, 15 and 20 K, with the crystal warmed to at least 20 K and then zero-field cooled between each measurement. The data shown include both the virgin and the return cycles of the curve.

Data obtained at 1.6 K along the ⟨110⟩ direction, showing the spin rotation in $FeTa_2O_6$, are provided in figure 10. An abrupt rise in the magnetization occurs at $H_{SF} = 69 \pm 1$ kOe. The value of the critical field required to induce the spin-flop was determined from the position of the sharp maximum in the λ peak associated with dM/dH (determined numerically), see figure 10, inset. Only the first family of antiferromagnetic planes, with spins parallel to **H**, seems to participate in the spin-flop. The second set of planes consists of moments directed perpendicular to the applied field. The contribution of these perpendicular moments can be identified for $H \leqslant H_{SF}$ as an approximately linear increase in the magnetization, associated

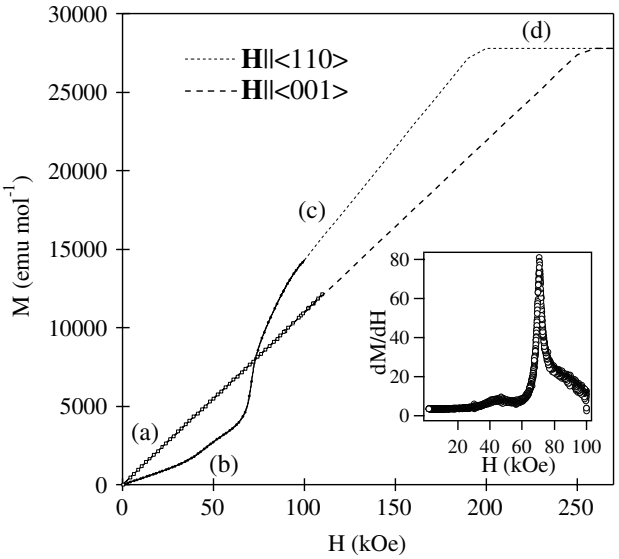

Figure 10. $FeTa_2O_6$ magnetization versus field for **H** applied parallel to the ⟨110⟩ and ⟨001⟩ directions at 1.6 K. The lower part of the graph $\mathbf{H} \ll 100$ kOe corresponds to the observed data. The dotted lines represent predictions for $\mathbf{H} \gg 100$ kOe. Inset is a plot of the derivative of the magnetization, d**M**/d**H**. Labels (a)–(d) refer to the spin configurations shown in figure 11.

with gradual canting of the moments towards **H**. This is shown schematically in figure 11(b). The behaviour of the spin-flop does not appear to be affected by the fields induced by the second set of moments, which indicates that any coupling between the two sets of perpendicular spins is likely to be weak.

At the critical field, $H_{SF} \simeq 69$ kOe, it becomes energetically more favourable to flip the sublattice of moments that is parallel to the field into a configuration similar to that pictured in figure 11(c). Assuming an effective moment of $5\mu_B$ per Fe atom, the saturation magnetization, M_{sat}, expected for this sample is around 27 800 emu mol^{-1}. Although we were not able to reach high enough fields with the current apparatus to witness the transition from the canted spin-flop phase to paramagnetic saturation (figure 11(d)), a prediction for the high-field behaviour is depicted in figure 10 as the dashed lines. These results have been calculated by assuming the simple linear relations,

$$\frac{\mathbf{M}_{\langle 110\rangle}}{\mathbf{H}} = \frac{M_{sat}}{(2H_e - H_a)} \tag{5}$$

and

$$\frac{\mathbf{M}_{\langle 001\rangle}}{\mathbf{H}} = \frac{M_{sat}}{(2H_e + H_a)}, \tag{6}$$

where H_e corresponds to the inter-sublattice exchange field and H_a the anisotropy field. This treatment predicts transitions from the spin-flop phase to saturation to occur at critical fields of around $H_{C\langle 110\rangle} = 194$ kOe and $H_{C\langle 001\rangle} = 254$ kOe for the [110] and [001] directions respectively (shown by the dashed lines in figure 10). The exchange and anisotropy fields are calculated to be $H_e = 112$ kOe and $H_a = 30$ kOe, respectively. The ratio $\alpha = H_a/H_e = 0.27$ is relatively large compared to most 2D structures. These values of H_e and H_a were used

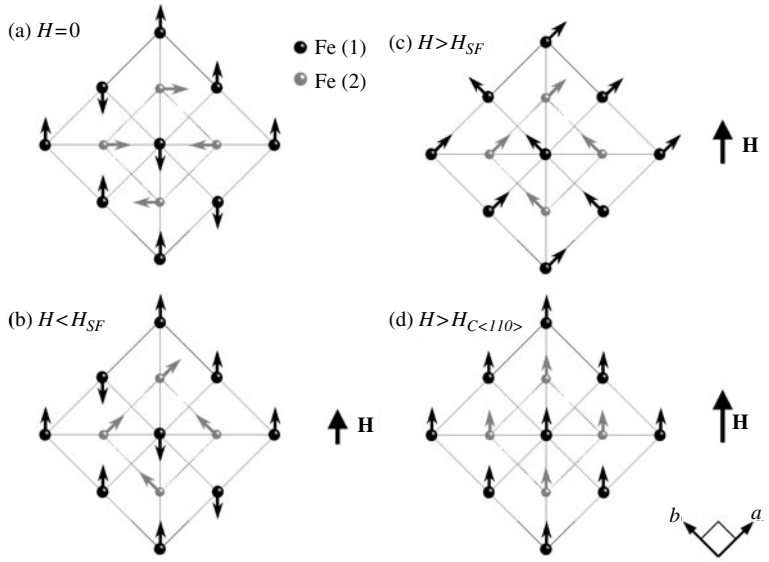

Figure 11. (a) $\mathbf{H} = 0$ configuration, (b) $\mathbf{H}\|[110]$ before spin-flop, (c) $\mathbf{H}\|[110]$ after spin-flop and (d) $\mathbf{H}\|[110]$ at saturation.

to predict a value for the critical field of the spin-flop transition:

$$H_{SF}^2 = 2H_e H_a - H_a^2. \tag{7}$$

The predicted value of H_{SF} is 76 kOe, while the observed value is 69 kOe. This is in reasonable agreement considering the simplicity of these approximations.

When the applied field is directed along the a or b axes (at 45° to the spin direction), the critical field required to rotate the moments occurs at ∼100 kOe. This value maps to a parallel component of applied field of ≃70 Oe which is in good agreement with $H_{SF} = 69 \pm 1$ kOe.

Our susceptibility results can also be compared to previous measurements performed upon polycrystalline samples by Zawislak *et al* [11]. Despite careful measurements, the averaging effects of the powder sample meant that Zawislak *et al* were not able to observe the spin-flop transition directly. They observed hysteresis above 60 kOe and predicted a spin-flop to occur at around $H_{SF} = 100$ kOe. In our data no hysteresis was associated with the spin-flop and $H_{SF} = 69$ kOe.

An explanation of the discrepancy between these two results can be found through a consideration of the large forces exerted upon the powder grains as they pass into the spin-flopped state. We suggest that these internal forces tend to re-orient the polycrystalline grains such that the spin direction and **H** are lying parallel. In experiments conducted with our single crystal, **H** was applied at an angle of $10 \pm 5°$ to the ⟨110⟩ direction. The crystal experienced a substantial torque at H_{SF}, which rotated the ⟨110⟩ direction to be exactly parallel to the applied field. Reorientation of the crystal occurred reproducibly each time the measurement was taken. We suggest that a similar reorientation of polycrystalline grains in the powder would have led to an apparent hysteresis in the data of Zawislak *et al* on passing through the spin-flop.

5. Neutron Laue diffraction

Neutron Laue diffraction patterns for $FeTa_2O_6$ were obtained using the recently commissioned Very-Intense Vertical Alignment Laue DIffractometer (VIVALDI), located at the high-flux reactor at the Institut Laue Langevin, Grenoble [17]. In this method neutron wavelengths in the waveband: 0.8–3.5 Å are scattered by the sample onto a cylindrical neutron-sensitive image plate, which subtends a solid angle of more than 2π sterad at the sample. The vertical alignment of VIVALDI makes it possible to investigate the behaviour of single crystals in a variety of sample environments.

In the current experiment VIVALDI was equipped with a long-tailed Orange cryostat and several 4 h exposures were collected at temperatures between 2 and 14 K. The Laue diffraction pattern observed at 2 K, where $FeTa_2O_6$ is antiferromagnetically ordered, is shown in figure 12(a). The clarity of the spot pattern confirms that the crystal is of excellent quality. At 2 K, the magnetic and structural diffraction patterns are observed simultaneously, with magnetic reflections occurring between pairs of rows of structural reflections. The triangular fans of weak scattering emanating from the centre of the figure arise due to a preferred orientation in the aluminium cryostat heat shields.

Figure 12(b) shows the Laue pattern observed at approximately $T_N = 8$ K. Here we find that the magnetic peaks have dissolved into extended streaks of diffuse magnetic scattering at low scattering angles. The diffuse scattering is revealed more clearly by the difference-Laue diffraction pattern shown in figure 13. The difference-Laue pattern has been calculated by subtraction of the images in figures 12(a) and (b). (The subtraction process serves to eliminate unwanted scattering from the cryostat, which is the same in both scans and similar in intensity to the magnetic diffuse scattering.) We find that the streaks of magnetic scattering correspond to the projections of 1D diffuse rods extending along the $\mathbf{c}^*$ direction in reciprocal space, perpendicular to the magnetic planes. Modelling of the diffuse scattering is complicated by chromatic overlap, and has been reserved for a future publication. Nonetheless, the Laue diffraction pattern of $FeTa_2O_6$ shown in figure 13 undisputibly verifies the existence of a 2D magnetic order.

6. Summary and discussion

In this paper we have demonstrated that $FeTa_2O_6$ is an $S = 2$ quasi 2D antiferromagnet ($T_N = 7.95 \pm 0.05$ K) with extensive short-range order in the *a*–*b* plane up to temperatures of at least four times T_N. In sections 3 and 4 the magnetic ordering and low-dimensional properties of $FeTa_2O_6$ were studied using heat-capacity and magnetization measurements. The heat-capacity data were of high quality and extended over a wider temperature range than previous reports, allowing the magnetic contribution to the heat capacity and magnetic entropy to be accurately estimated. We find that approximately 73% of the magnetic entropy of $FeTa_2O_6$ is lost above T_N due to short-range order effects.

Our studies of the susceptibility and **M**–**H** dependence along various directions in the single crystal show that there is a high magnetic anisotropy between the *a*–*b* plane and the *c* direction. Extensive in-plane short-range correlations are present up to at least 35 K. We find that the bulk crystal contains approximately equal populations of spins along the four symmetry equivalent ⟨110⟩ directions. This would be consistent with the presence of equal populations of magnetic domains, and/or a rotation of the spin direction by 90° on translation from one magnetic plane to the next (in agreement with the local co-ordination of the oxygen atoms). With **H** applied parallel to the *a*–*b* plane a spin-flop transition is also observed.

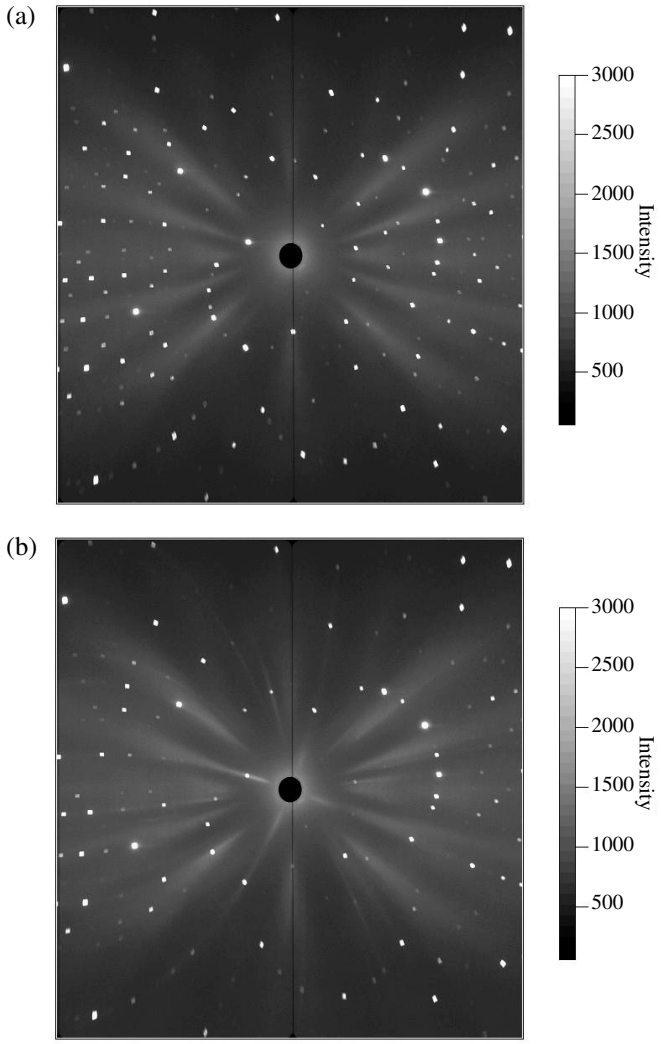

Figure 12. Neutron Laue diffraction patterns observed for a single crystal of $FeTa_2O_6$. The image plates are mounted inside a cylinder 40 cm long and 100 cm in circumference. The regions shown are 40 cm high and 40 cm around the circumference centred about the transmitted beam. (a) At 2 K both the magnetic and structural Bragg peaks are observed. The triangular fan-shaped intensity radiating from the centre of the image—the direction of the transmitted beam—results from scattering from the aluminum cryostat. (b) At 8 K only the structural reflections remain, but streaks of magnetic diffuse scattering are visible at low **Q**.

Single-crystal neutron-Laue measurements directly confirming the presence of 2D short-range order in $FeTa_2O_6$ were presented. The neutron-Laue photograph of a single crystal $FeTa_2O_6$, obtained at approximately T_N, shows clear streaks of 1D magnetic diffuse scattering extending along the $\mathbf{c}^*$ direction in reciprocal space, perpendicular to the magnetic Fe^{2+} planes.

Complementary monochromatic neutron and time-of-flight experiments investigating the magnetic structure and temperature evolution of short-range correlations in $FeTa_2O_6$ have been performed in more detail and will be published separately.

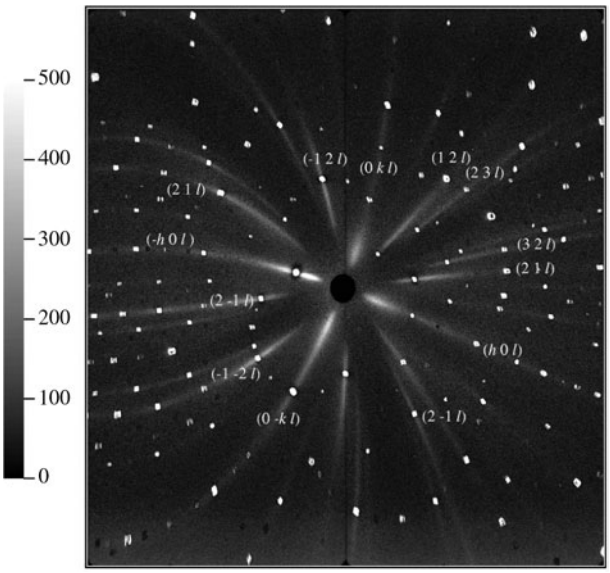

Figure 13. The difference Laue pattern obtained for a single crystal of $FeTa_2O_6$ by subtraction of figures 12(a) and (b). Streaks of 1D diffuse magnetic scattering can be clearly observed. The trajectories of the most intense 1D rods through reciprocal space are labelled. The existence of diffuse scattering rods in the $\mathbf{c}^*$ direction provides direct confirmation of 2D magnetism in $FeTa_2O_6$ in the region of T_N.

Acknowledgments

The authors are grateful to J Key and M Davis (University of Warwick) for technical assistance and the Engineering and Physical Sciences Research Council (EPSRC), UK, for financial support.

References

[1] Zawislak L I, da Cunha J B M, Vasquez A and dos Santos C A 1995 *Solid State Commun.* **94** 345
[2] Eicher S M, Greeden J E and Lushington K J 1986 *J. Solid State Chem.* **62** 220
[3] Saes M, Raju N P and Greedan J E 1998 *J. Solid State Chem.* **140** 7
[4] Chung E M L, McIntyre G J, Lees M R, Balakrishnan G, Visser D, Paul D M and Wilkinson C 2002 *Institut Laue–Langevin Annual Report Scientific Highlights* p 16
[5] Goldschmidt V M 1926 *Skr. Nor. Vidensk. Acad. Oslo* **1** 17
[6] Hansen S, Landa-Cánovas A, Ståhl K and Nilsson J 1995 *Acta Crystallogr.* A **51** 514
[7] de Jongh L J and Miedema A R 1974 *Adv. Phys.* **23** 1
[8] Takano M and Takada T 1970 *Mater. Res. Bull.* **5** 449
[9] Weitzel H and Klein S 1977 *Acta Crystallogr.* A **30** 380
[10] Bernier J C 1971 *Compt. Rendu.* C **273** 1166
[11] Zawislak L I, Fraga G L F, da Cunha J B M, Schmitt D, Carrico A S and dos Santos C A 1997 *J. Phys.: Condens. Matter* **9** 2295
[12] Muraoka Y, Idogaki T and Uryu N 1988 *J. Phys. Soc. Japan* **57** 1758
[13] Fan C and Wu F Y 1969 *Phys. Rev.* **179** 560
[14] Tanaka I, Kanai H and Kojima H 1985 *J. Crystal Growth* **73** 175
[15] Fisher M E 1962 *Phil. Mag.* **7** 1731
[16] Shapira Y and Foner S 1970 *Phys. Rev.* B **1** 3083
[17] Wilkinson C, Cowan J A, Myles D A A, Cipriani F and McIntyre G J 2002 *Neutron News* **13** 37